Comparison of the Fermi-surface topologies of κ-(BEDT-TTF)$_2$Cu(NCS)$_2$ and its deuterated analogue

R.S. Edwards[1], A. Narduzzo[1], J. Singleton[1,2], A. Ardavan[1] and J.A. Schlueter[3]
[1] *Oxford University Department of Physics, Clarendon Laboratory, Parks Road, Oxford OX1 3PU, United Kingdom.*
[2] *National High Magnetic Field Laboratory, Los Alamos National Laboratory, TA-35, MS-E536, Los Alamos, NM87545, USA*
[3] *Materials Science Division, Argonne National Laboratory, Argonne, Illinois 60439, USA*

We have measured details of the quasi one-dimensional Fermi-surface sections in the organic superconductor κ-(BEDT-TTF)$_2$Cu(NCS)$_2$ and its deuterated analogue using angle-dependent millimetre-wave techniques. There are significant differences in the corrugations of the Fermi surfaces in the deuterated and undeuterated salts. We suggest that this is important in understanding the inverse isotope effect, where the superconducting transition temperature rises on deuteration. The data support models for superconductivity which invoke electron-electron interactions depending on the topological properties of the Fermi surface.

PACS numbers: 71.18.+y, 71.27.+a, 72.80.Le, 74.70.-b, 78.70.Gq

The nature of the superconducting groundstate in quasi-two-dimensional charge-transfer salts such as κ-(BEDT-TTF)$_2$Cu(NCS)$_2$ has attracted much recent experimental [1, 2, 3, 4] and theoretical [5, 6, 7, 8, 9] interest. The majority of the experimental data suggest that the superconductivity is not describable by a simple BCS-like, phonon-mediated approach (for a review, see Refs. [4, 10] and refs. therein). Consequently, a number of the theoretical treatments invoke pairing mediated by electron-electron interactions and/or antiferromagnetic fluctuations [5, 6, 7, 8, 9]. In such a scenario, the "nestability" of the Fermi surface is an important consideration; it is expected that alterations of the Fermi-surface topology will affect the superconducting transition temperature [5, 6, 7, 8, 9].

In this context, the observation of a "negative isotope effect" in κ-(BEDT-TTF)$_2$Cu(NCS)$_2$ may be of great importance [11, 12]; on replacing the terminal hydrogens of the BEDT-TTF molecule in κ-(BEDT-TTF)$_2$Cu(NCS)$_2$ by deuterium, it was found that an increase ($\Delta T_c \approx 0.3$ K) in the superconducting critical temperature T_c occurred [11, 12]. By contrast, isotopic substitutions of other atoms in the BEDT-TTF molecule or in the anion layer produce a very small, normal isotope effect or no significant isotope effect at all, respectively [12]. In this paper we describe millimetre-wave measurements which compare the Fermi surfaces of deuterated and conventional samples of κ-(BEDT-TTF)$_2$Cu(NCS)$_2$. The data suggest that it is primarily the changes in the topology of the Fermi surface brought about by deuteration that cause the observed isotope effect, supporting models for superconductivity involving pairing via electron-electron interactions [5, 6, 7, 8, 9].

The Fermi surface of κ-(BEDT-TTF)$_2$Cu(NCS)$_2$ comprises a quasi-two-dimensional (Q2D) pocket (the α pocket) and a pair of quasi-one-dimensional (Q1D) sheets [13]; it is similar to that used by Pippard to predict magnetic breakdown [14]. It is known that the α pocket is hardly affected by deuteration [4], and so our measurement concentrates on the Q1D sheets. Fermi-surface traversal resonances (FTRs) [15, 16] (i.e. resonances in the high-frequency conductivity caused by magnetic-field-induced motion of quasiparticles across the Fermi sheets) are used to infer the corrugations of the sheets.

The experiments involved single crystals of κ-(BEDT-TTF)$_2$Cu(NCS)$_2$ ($\sim 0.7 \times 0.5 \times 0.1$ mm^3; mosaic spread $\lesssim 0.1°$), produced using electrocrystallization [11, 12]. In some of the crystals, the terminal hydrogens of the BEDT-TTF molecules were isotopically substituted by deuterium; we refer to the deuterated samples as d8, and conventional hydrogenated samples as h8. A single sample is mounted at the centre (in a magnetic field antinode) of a rectangular cavity of inner dimensions $1.55 \times 3.10 \times 6.00\,\mathrm{mm}^3$ resonating at 72 GHz in the TE_{102} mode [15]; the oscillating H-field lies within the sample's Q2D (**b**, **c**) planes. In this configuration, the effective skin depth is very large, and the GHz fields penetrate the bulk of the sample [15]. The cavity can be rotated with respect to the external quasistatic magnetic field **B** so as to vary the angle θ between **B** and the normal to the sample's Q2D planes [15]; the normal to the Q2D planes is the $\mathbf{a}^*$ direction of the reciprocal lattice [17, 18]. In addition, the sample can be turned about $\mathbf{a}^*$ within the cavity, so as to vary the plane of rotation, defined by the azimuthal angle ϕ [15]. The angles θ and ϕ and their relationship to the Q1D sheet of the Fermi surface are given in the inset to Fig. 1.

Experiments were carried out on samples of d8 κ-(BEDT-TTF)$_2$Cu(NCS)$_2$for angles $-70° \leq \theta \leq 70°$ for four different azimuthal angles ϕ. Fig. 1 shows results for an azimuthal angle of $\phi = 5°$ for θ values between 0° and 70° in 5° steps, at a temperature of 1.5 K. At low fields (around 4 T at $\theta = 0°$) one absorption can be seen (thick dashed line in Fig. 1). This is related to the superconducting to normal transition of the sample [3]; it follows the θ dependence of the upper critical field, $\mu_0 H_{c2}$, which varies approximately as $1/\cos\theta$ [19]. At high field magnetic quantum oscillations are observed, indicating that the sample is pure; the angular behaviour of the frequency F of the oscillations ($F \propto 1/\cos\theta$) pro-

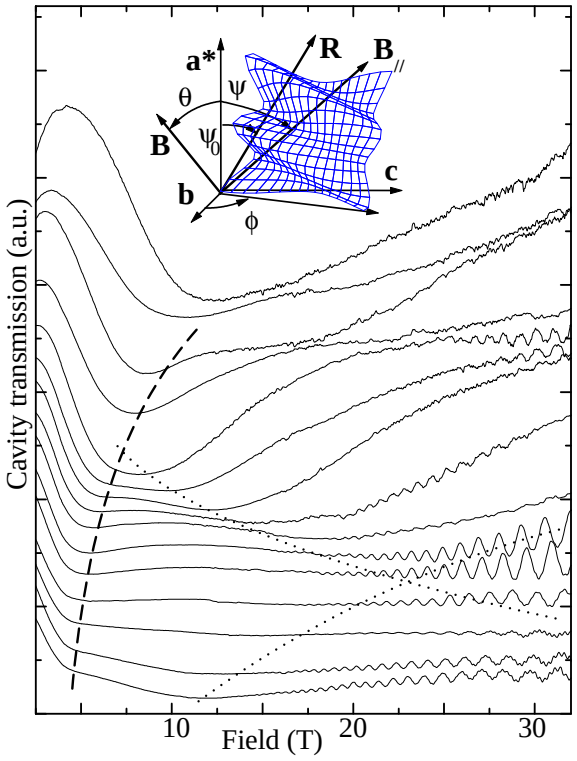

FIG. 1: Transmission of a cavity loaded with a d8 κ-(BEDT-TTF)$_2$Cu(NCS)$_2$ sample versus magnetic field. The temperature was 1.5 K and $\phi = 5^\circ$. Field sweeps at angles from $\theta = 0^\circ$ (bottom) to 70° (top) in 5° steps are shown, normalised and offset for clarity. The thick dashed line shows the position of a feature associated with the superconducting-to-normal transition, while the fine dashed lines show the FTRs. Inset: the relationship between the coordinates $\mathbf{B}$, θ and ϕ, the component of the field $\mathbf{B}_{||}$ and the angle ψ. $\mathbf{R}$ indicates the axis of the Fermi-surface corrugation.

vides a check of the angle θ [10]. At some θ, magnetic breakdown oscillations, caused by tunnelling between the Q2D and Q1D Fermi-surface sections, are superimposed on the lower frequency oscillations caused by the Q2D pocket [10, 15]. At intermediate fields there are two broad absorptions [20] (fine dashed lines); their (θ, ϕ) dependence (see below) allows them to be unambigously attributed to FTRs caused by the Q1D sheets.

The field positions of the FTRs were recorded for all angles studied. In order to analyse the FTRs, the experimental coordinates $\mathbf{B}$, θ and ϕ must be converted into the component of the field $\mathbf{B}_{||}$ within the plane of the Q1D Fermi-surface sheets, and the angle ψ between the normal to the sample's Q2D planes and $\mathbf{B}_{||}$ (see Fig. 1, inset) [15]. This done via the equations [15]

$$\begin{aligned} B_{||} &= B\sqrt{\sin^2\theta\cos^2\phi + \cos^2\theta}, \\ \tan\psi &= \tan\theta\cos\phi. \end{aligned} \quad (1)$$

Each corrugation of the Q1D Fermi sheets is expected to give rise to a FTR with the ψ dependence [15, 21],

$$\frac{\omega}{B_{||}} = A\sin(\psi - \psi_0). \quad (2)$$

Here, ω is the angular frequency of the millimetre-waves, A is a constant depending on details of the Fermi surface [15], and ψ_0 defines the axis of the corrugation $\mathbf{R}$ (Fig. 1, inset). As the millimetre-wave frequency is held constant, the FTRs should lie on sinusoidal "arches" when $1/B_{||}$ is plotted as a function of ψ [15].

Fig. 2 shows the FTR positions plotted in terms of $1/B_{||}$ and ψ. Apart from a region close to $\psi = +100^\circ$ where the feature associated with the superconducting to normal transition obscures the FTRs at some ϕ, making the exact position difficult to gauge, the data lie on two "arches", shown as curves (Fig. 2); the curves were obtained by fitting the data to Eqn. 2. This indicates that the Q1D Fermi surface of d8 κ-(BEDT-TTF)$_2$Cu(NCS)$_2$ has two distinct corrugations, with their axes $\mathbf{R}_1$ and $\mathbf{R}_2$ at angles $\psi_0 = 17.9^\circ \pm 2.0^\circ$ and $39.8^\circ \pm 2.0^\circ$ to $\mathbf{a}^*$ respectively.

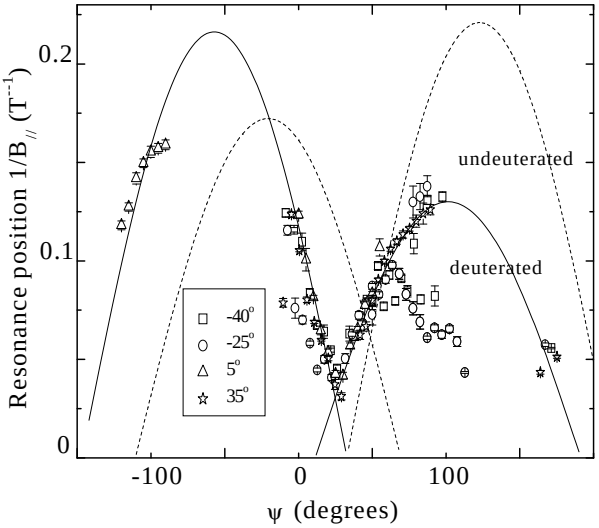

FIG. 2: The field positions of the resonances in d8 κ-(BEDT-TTF)$_2$Cu(NCS)$_2$ in FTR coordinates. Data for four different azimuthal angles studied at 1.5 K are shown; squares $\phi = -40^\circ$; circles $\phi = -25^\circ$; triangles $\phi = 5^\circ$; stars $\phi = 35^\circ$. Two curves (solid lines) show the fits to the resonances using Eqn 2. The dotted lines show equivalent fits to data from h8 κ-(BEDT-TTF)$_2$Cu(NCS)$_2$. For clarity the data points have been omitted (see Ref. [15] for representative data).

Equivalent experiments were carried out in h8 κ-(BEDT-TTF)$_2$Cu(NCS)$_2$. (Some representative data are shown in Ref. [15]). Again, the resonance positions lie on two "arches" (shown in Fig. 2), implying that the Q1D Fermi surface of h8 κ-(BEDT-TTF)$_2$Cu(NCS)$_2$ has two distinct corrugations [15]. In this case, the corrugation axes $\mathbf{R}_1$ and $\mathbf{R}_2$ are at angles $\psi_0 = 21.2^\circ \pm 2.0^\circ$ and $-20.8^\circ \pm 2.0^\circ$ to $\mathbf{a}^*$ respectively. The data for both samples are summarised in Table I.

κ-(BEDT-TTF)$_2$Cu(NCS)$_2$ has a monoclinic crystal structure with the crystallographic **a**-axis at an angle of 20.3° to the normal to the Q2D planes (**a***) [17]; in this respect, the crystal structures of d8 and h8 κ-(BEDT-TTF)$_2$Cu(NCS)$_2$ appear identical [18]. Within tight-binding bandstructure, the corrugation axes of a Fermi surface usually relate to the primitive lattice translation vectors of the *real-space* lattice [22]. Rather than work in terms of the angle ψ_0, which defines the directions of the corrugation axes with respect to **a***, it is more useful to use the angle Ψ_0, which relates to the real-space vector **a**. Once this is done (Table I), it is plain that the corrugation axis $\mathbf{R}_1$ in both the d8 and h8 samples lies very close to the **a** (interlayer) direction. By contrast, the direction of $\mathbf{R}_2$, the second corrugation axis, differs; with reference to the primitive lattice translation vectors

$$\mathbf{T}_{mn} = m\mathbf{a} + n\mathbf{c} \tag{3}$$

where m and n are integers, we find that in d8, $\mathbf{R}_2$ is very close in direction to $\mathbf{T}_{2\bar{1}}$, whereas in h8, it is close in direction to $\mathbf{T}_{11}$ (Table I). The reasons for the dominance of these particular directions are unclear; however, interlayer coupling through the anion layer is presently poorly understood at a molecular-orbital level. It is possible that a variety of overlap-pathways may be operative and that the choice of dominant overlap-pathway through the anion layer depends very sensitively on the exact coordinates of the terminal end of the BEDT-TTF molecule. In this context, it will be very useful to have high-resolution structural experiments which address the detailed differences between h8 and d8 at low temperatures [18].

Finally, it is interesting to work out the relative amplitudes of the corrugations in h8 and d8 κ-(BEDT-TTF)$_2$Cu(NCS)$_2$. Models of FTR allow one to relate the intensity of the FTR to the amplitude of the Fermi-surface corrugation [21]. Measurements of the d.c. transport properties of d8 and h8 κ-(BEDT-TTF)$_2$Cu(NCS)$_2$ suggest that the transfer integral $t_\perp$ in the **a** direction is very similar in the two materials ($t_\perp \approx 0.04$ meV) [13]. This implies that the Fermi-surface corrugations along $\mathbf{R}_1$ should be very similar in d8 and h8 [13]; in d8 and h8 samples with equal volume the corresponding FTRs should have the same intensity [21]. The average intensities I of each FTR for $\theta = 0°$ are shown in Table I. As the samples are of different size, the intensities of the FTRs have been normalised to that of the FTR corresponding to $\mathbf{R}_1$.

Using the periodicity in k-space [17], the relative intensities of the FTRs, and the orientations Ψ_0 of $\mathbf{R}_1$ and $\mathbf{R_2}$, it is possible to make a comparison of the Q1D Fermi sheets for both materials. Fig. 3 shows these representations, with the corrugations, assumed sinusoidal, shown at the same scale. This scale is chosen so that the differences between d8 and h8 are clear; in reality, the small measured value of $t_\perp$ [13] suggests that the corrugations will be on an extremely small scale.

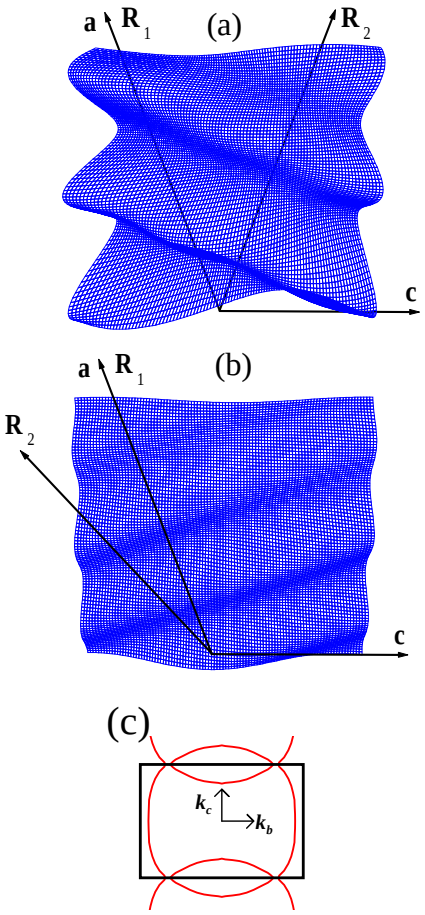

FIG. 3: (a) Representation of the Q1D Fermi-sheet topology in h8 κ-(BEDT-TTF)$_2$Cu(NCS)$_2$ derived from the fits to the FTR data; (b) the same for d8 κ-(BEDT-TTF)$_2$Cu(NCS)$_2$ plotted at the same scale. The corrugations have been greatly enhanced for clarity. (c) Plan view of the Fermi surface of κ-(BEDT-TTF)$_2$Cu(NCS)$_2$, showing the Q2D pocket and Q1D sheets [13]; (a) and (b) represent side views (*i.e.* looking along $\mathbf{k_b}$) of the Q1D sheets.

Despite an intensive search, no features attributable to cyclotron resonance (CR) due to the Q2D Fermi-surface pocket were observed in either d8 or h8, in agreement with previous studies [15]. The response of our cavity system is dominated by the interlayer component of the sample's high-frequency conductivity [15, 16]. Fermi-surface sections with more complex corrugations in the interlayer direction will dominate the high-frequency interlayer conductivity [21]; recent resistivity measurements of κ-(BEDT-TTF)$_2$Cu(NCS)$_2$ suggest that the corrugations of the Q2D pocket are simpler and more regular than those of the Q1D sheets [13], perhaps explaining the absence of CR. Similarly, the *in-plane* corrugations of the Q1D sheet (Fig. 3(c)) will have little effect on the high-frequency *interlayer* conductivity [21], and therefore do not result in detectable FTRs.

It is obvious that there is a difference between the Q1D Fermi sheets of the two materials, with the corrugations

	d8 $\mathbf{R}_1$	d8 $\mathbf{R}_2$	h8 $\mathbf{R}_1$	h8 $\mathbf{R}_2$
A/ω	0.198 ± 0.004	$0.131 \pm .002$	0.204 ± 0.004	0.168 ± 0.004
ψ_0	$17.9 \pm 2.0^\circ$	$39.8 \pm 2.0^\circ$	$21.2 \pm 2.0^\circ$	$-20.8 \pm 2.0^\circ$
Ψ_0	$-2.4 \pm 2.0^\circ$	$19.5 \pm 2.0^\circ$	$0.9 \pm 2.0^\circ$	$-41.1 \pm 2.0^\circ$
$\mathbf{T}_{mn}$	$\mathbf{T}_{10}$	$\mathbf{T}_{2-1}$	$\mathbf{T}_{10}$	$\mathbf{T}_{11}$
I	1	0.34 ± 0.06	1	6 ± 2

TABLE I: The values for A/ω (see Eqn. 2), ψ_0 (angle of corrugation axis with respect to $\mathbf{a}^*$) and Ψ_0 (angle of corrugation axis with respect to $\mathbf{a}$) for each of the FTRs seen in d8 and h8 κ-(BEDT-TTF)$_2$Cu(NCS)$_2$. Also shown are the vectors $\mathbf{T}_{mn}$ which define the directions of the corrugation axes $\mathbf{R_1}$ and $\mathbf{R}_2$ (see Eqn. 3). I is the average intensity of the FTR at $\theta = 0^\circ$ normalised as described in the text.

in h8 being stronger; the dominant corrugation has axis $\mathbf{R}_2$, at -41.1° to $\mathbf{a}$. By contrast, the corrugations in d8 κ-(BEDT-TTF)$_2$Cu(NCS)$_2$ are weaker, and are dominated by that with axis $\mathbf{R}_1$ lying along $\mathbf{a}$. This suggests that the Fermi surface of d8 κ-(BEDT-TTF)$_2$Cu(NCS)$_2$ would be more amenable to nesting than that of h8.

Our data support models for superconductivity such as those of Refs. [6, 7]. In these, the pairing of electrons is mediated by electron-electron interactions which depend on the "nestability" of the Fermi-surface; hence they predict a T_c which is sensitive to the details of the Fermi-surface topology. The difference between the Q1D Fermi sheets of d8 and h8 κ-(BEDT-TTF)$_2$Cu(NCS)$_2$ measured using FTR can thus explain the isotope effect; the Q1D Fermi sheets in the d8 samples are less corrugated (and therefore more nestable), leading to a higher T_c.

In summary, we have measured details of the Fermi-surface topology of the deuterated organic superconductor κ-(BEDT-TTF)$_2$Cu(NCS)$_2$, and compared them with equivalent measurements of the undeuterated salt. We find that the quasi-one-dimensional Fermi-surface sheets are significantly more corrugated in the undeuterated salt, perhaps explaining the "inverse isotope effect" observed on deuteration. Our data support models for exotic d-wave superconductivity in the organics which invoke electron-electron interactions depending on the topological properties of the Fermi surface.

This work is supported by EPSRC (UK). NHMFL is supported by the US Department of Energy (DoE), the National Science Foundation and the State of Florida. Work at Argonne is sponsored by the DoE, Office of Basic Energy Sciences, Division of Materials Science under contract number W-31-109-ENG-38. We thank Stephen Hill and Stephen Blundell for constructive comments.

[1] K. Izawa *et al.*, Phys. Rev. Lett. **88**, 027002 (2002).
[2] H. Elsinger *et al.* Phys. Rev. Lett. **84** 6098 (2000).
[3] S.O. Hill *et al.*, Phys. Rev. Lett. **86**, 3451 (2001); J.M. Schrama *et al.*, ibid., 3452.
[4] T. Biggs *et al.*, J. Phys.: Condens. Matter **14**, L495 (2002).
[5] J. Schmalian, Phys. Rev. Lett. **81** 4232 (1998).
[6] K. Kuroki *et al.* preprint cond-mat 0108506 (2001).
[7] R. Louati *et al.* Phys. Rev. B **62**, 5957 (2000).
[8] K. Kuroki and H. Aoki, Phys. Rev. B **60**, 3060 (1999).
[9] Won-Min Lee, Solid State Commun.**106**, 601 (1998).
[10] J. Singleton and C. Mielke, Contemp. Phys. **43**, 150 (2002).
[11] A. M. Kini *et al.* Physica C **264** 81 (1996)
[12] J. A. Schlueter *et al.* Physica C **351** 261 (2001).
[13] J. Singleton *et al.* Phys. Rev. Lett. **88**, 037001 (2002).
[14] A.B. Pippard, Proc. Roy. Soc. A **270**, 1 (1962).
[15] J.M. Schrama *et al.*, J. Phys.:Cond. Matt. **13**, 2235 (2001).
[16] A. Ardavan *et al.*, Phys. Rev. Lett. **81**, 713 (1998).
[17] H. Urayama *et al.* Chem. Lett. **1988**, 463 (1988).
[18] Y. Watanabe *et al.* Synth. Met. **86** 1917 (1997).
[19] M-S. Nam *et al.* J. Phys.: Cond. Matt. **11**, L477 (1999).
[20] For most θ, these absorptions occur well away from the regions of significant magnetic breakdown. Hence, the quasiparticle motion across the Q1D sheets is decoupled from that on the Q2D pocket; resonances can be unambiguously associated with either the Q1D or Q2D sections of the Fermi surface.
[21] A. Ardavan *et al.* Phys. Rev. B, **60**, 15500 (1999); S.J. Blundell *et al.* Phys. Rev. B **55** R6129 (1997).
[22] N.W. Ashcroft and N.D. Mermin, *Solid State Physics*, Saunders (1976).